An Exercise in demonstrating Time Dilation

Jun Rui Ting*, Kushagra Shrivastava*, Lu Xixun*

* Department of Physics, National University of Singapore, Science Drive 4, National University of Singapore, 119077, Singapore

For the fulfillment of the PC1101 Frontiers of Physics term paper

We would like to extend our heartfelt thanks, gratitude and appreciation to **A/Prof. Phil CHAN Aik Hui, Mr. KUANG Jianhong** and the Department of Physics in the National University of Singapore for their guidance and unwavering support for the completion of this term paper.

Jun Rui, Kush & Xixun

Abstract

Einstein's Theory of Special Relativity, a cornerstone of modern physics, predicts time dilation, where the passage of time, as observed by an observer, varies with relative motion. Confirming this theory, the detection of muons—relativistic particles—becomes crucial. In this study, we utilized the CosmicWatch Muon Detector to measure muon counts at various elevations. The theoretical muon count rate at ground level was then calculated and juxtaposed with the experimental count at ground level. Additionally, we compared the effects of additional shieldings (aluminum foil, water) on the observed muon count rate. This experiment successfully demonstrates the relativistic effect on the muon lifetime, providing empirical confirmation of Einstein's Theory of Special Relativity.

Introduction

Einstein's Theory of Special Relativity,[1] introduced in 1905, revolutionized the notion of space and time. It proposes two fundamental postulations: length contraction and time dilation. Length contraction posits that as an object's speed approaches the speed of light (c), its length appears to shrink along its direction of motion when observed from a slower-moving frame. This phenomenon challenges the classical Galilean and Newtonian relativistic interpretation of absolute space. Likewise, time dilation suggests that time is not absolute but instead relative to an observer's motion. As an object moves at high speeds, elapsed time observed by the object slows down compared to an observer at rest. Together, these postulates reveal the intricate relationship between space and time, redefining our understanding of the fabric of the universe.

To this, ground-based detection methods have played a pivotal role in demonstrating Einstein's Theory of Special Relativity. By carefully measuring physical phenomena, such as the decay of cosmic ray muons, at varying altitudes or relative velocities on the Earth's surface, direct first-hand empirical evidence can be obtained to corroborate the effects predicted by time dilation and length contraction.[2]

Muons, the primary focus of this investigation, are subatomic particles belonging to the family of leptons, alongside electrons and neutrinos. They are similar to electrons but are comparatively approximately 207 times more massive. Muons, formerly known as *μ-mesons*, are primarily created in high-energy cosmic ray interactions with the Earth's atmosphere. However, compared to electrons, they have significantly shorter mean lifetimes, originally taken to be 2.4 μs in Rossi and Hall's seminal paper on ground-based muon decay detection,

the mean lifetimes of muons have been measured more recently to significantly better precision. As it stands, current measurements of mean lifetimes of muons is $2.1969811(22) \times 10^{-6}$s.[3]

A result of the collision of high-energy cosmic rays with particles in Earth's atmosphere, muons created through this interaction have velocities close to the speed of light. As such, they experience significant time dilation effects. This phenomenon makes muons an invaluable tool in experimental physics, astrophysics, and particle physics research, as they provide concrete evidence for Einstein's theory and thus help us better understand the fundamental interactions of the universe. Muons have thus become crucial in a variety of experiments, such as the aforementioned Rossi and Hall's 'Rate of Decay of Mesotrons with Momentum', comparing muon decay rates at varying altitudes to validate the predictions of Einstein's Special Theory of Relativity.

Devices that can detect Muons are being readily made available for students as a freely and openly accessible introduction to particle physics and astrophysics experimentation. The device used in this project is CosmicWatch, a Desktop Muon Detector developed by the Massachusetts Institute of Technology (MIT) and National Center for Nuclear Research (NCBJ).[4] It consists of light-sensing device attached to an extruded slab of plastic scintillator, altogether connected to an Arduino Nano. This allows it to detect particles, particularly muons, in individual discrete events.

In this project, the CosmicWatch Muon Detector was used to demonstrate Einstein's Theory of Special Relativity's prediction of time dilation. This was achieved by collecting muon counts at an accessible elevated location, *Singapore's Marina Bay Sands Observation Deck* (at 195.0m), and at varying 'ground' levels. The difference in the theoretical muon count and the observed muon count at an altitude is a proof of Einstein's theory of special relativity.

Materials & Methods

Building CosmicWatch Desktop Muon Detector

Following the circuit design described by Axani et al.[5], components were soldered onto three PCBs: Main PCB, SD Card PCB, and the SiPM PCB. A BNC receptacle, reset button, coincidence connection, temperature sensor, 6-pin connector, LED, 8-pin header, 4-pin OLED connector, and an Arduino Header was soldered onto the Main PCB. A logic converter and a microSD card socket was soldered onto the SD Card PCB. The 8-pin header was then used to

connect and solder the Main PCB and the SD Card PCB together. The SiPM was soldered on the SiPM PCB with a 6-pin header. An Arduino Nano was then connected to the Arduino header on the Main PCB. Figure 1 shows the front and backside of these PCBs.

The Plastic Scintillator was covered with a reflective aluminum sheet and optically isolating black electrical tape. A 5 cm by 5 cm square region was cut out at the center on one side of the Scintillator (as shown in Figure 2Ai and 2Aii) for the SiPM. The Plastic Scintillator and the SiPM PCB were placed in plastic trays that can be joined together, as shown in Figure 2Bi and 2Bii, ensuring that the 5 cm by 5 cm opening in the scintillator aligns with the SiPM. To prevent misalignment, the SiPM PCB on tray attached with the Plastic Scintillator on tray were then taped together using optically isolating black electric tape (Figure 1C). This piece was then connected to the Main PCB by joining the 6-pin header and the 6-pin connector.

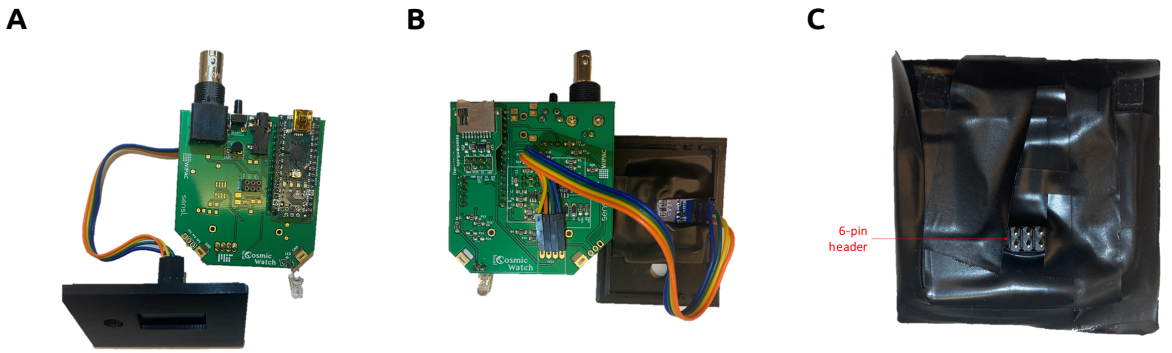

Figure 1: (**A**) and (**B**) shows the front and the back of the Main PCB connected with the SD Card PCB and the OLED screen taped with the plastic casing, respectively. (**C**) shows the taped plastic scintillator and the SiPM.

The entire device was inserted into a plastic casing, ensuring precise alignment of the OLED display, LED, USB mini input, SD card slot, reset button, and the BNC receptacle with their corresponding pre-cut slots in the plastic casing. The finalized device is depicted in Figure 3.

The Arduino Code was loaded into the device (for either the OLED or the microSD card). The device was then powered by a powerbank and data was collected. The device that was soldered did not function as expected, and therefore a pre-soldered device was used for Data Collection instead.

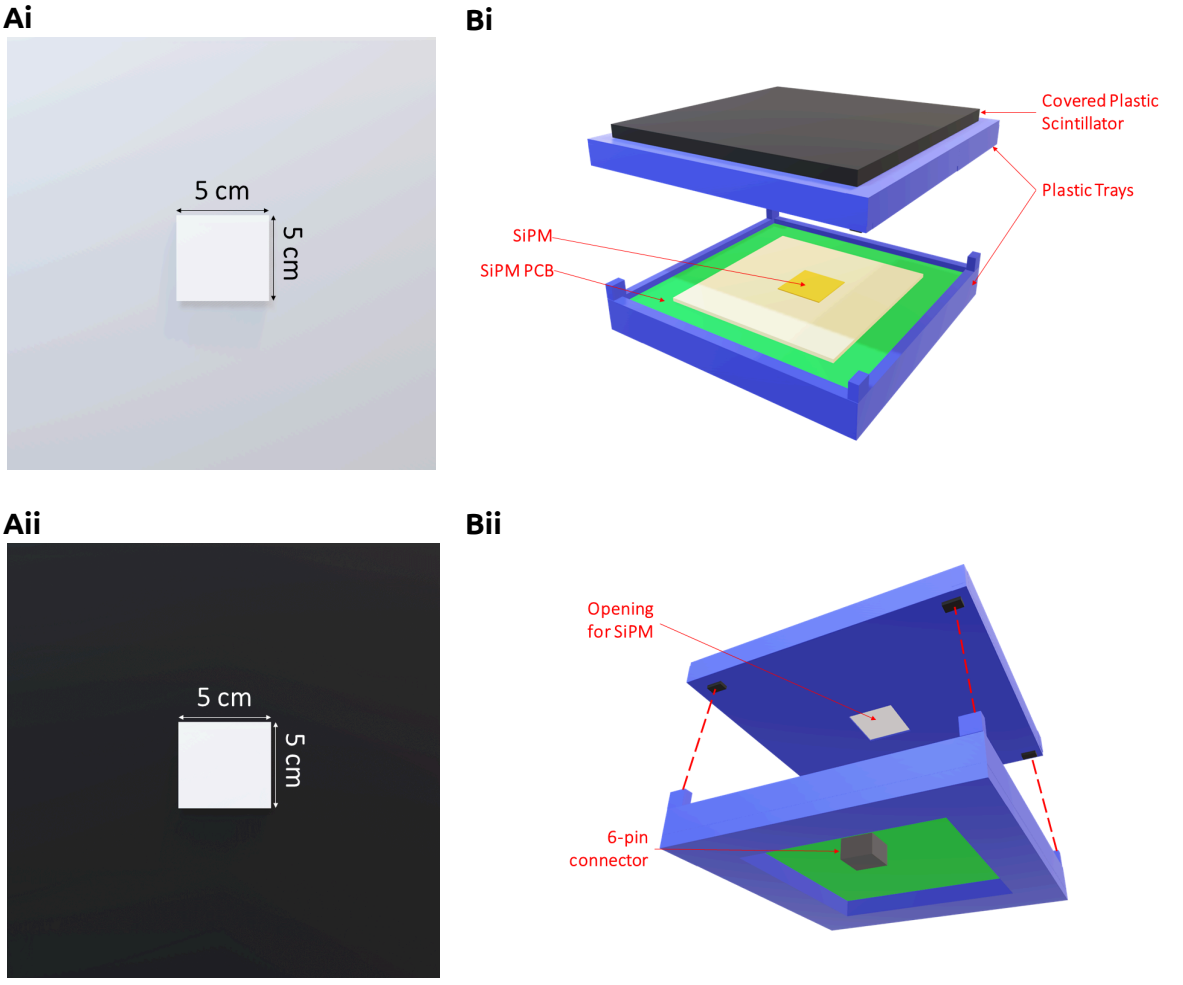

Figure 2: (**Ai**) Plastic Scintillator with aluminum foil covering and a 5 cm by 5 cm opening. (**Aii**) Plastic Scintillator with aluminum foil and black tape covering and a 5 cm by 5 cm opening. (**Bi**) The assembled SiPM and Scintillator module's top view. (**Bii**) The assembled SiPM and Scintillator module's bottom view. The dotted lines represent in which groove (on the Plastic Scintillator tray) each peg will fix (on the SiPM PCB tray). *[All 3D models were made using Microsoft Paint3D]*

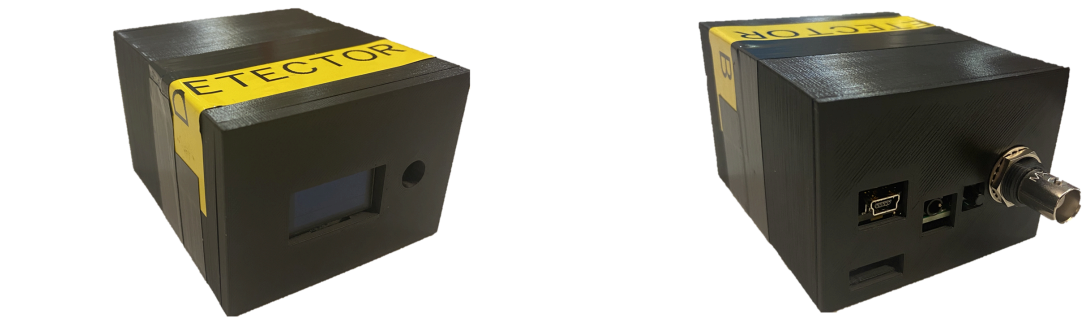

Figure 3: (**A**) and (**B**) shows the front and the back of the detector respectively. As seen, the OLED screen, LED, microSD Card Slot, BNC receptacle, reset button, micro USB slot, and the coincidence connection are aligned with the grooves made in the plastic casing.

Data Collection

Before commencing data collection, a location was carefully selected away from potential sources of electromagnetic interference, such as power plugs and buildings. To ensure the absence of underground wires in the data collection area, the magnetic field of the location was tested. The measurements at all collection points consistently registered around 20μT, as determined using the Magnetometer in the Physics Toolbox Suite.[6]

The elevations of each of the locations chosen were estimated from its relative elevation from 'ground level'. The elevation of each of the 'ground levels' were retrieved from a topographical map of Singapore.[7] The elevation and the total collection time for each of the data collection locations are shown in Table 1.

Before saving the data, the OLED display code was uploaded to the Arduino Nano to ensure the CosmicWatch is functional. Then, the microSD card code was uploaded and the data collection was started.

Table 1: Summary of data collection locations

Location	Elevation (above Sea Level) [m]	Total Dataset Collection Time [s]
UTown Green	4.00 ± 0.50	18359.408
MBS Ground Level	15.00 ± 3.00	2790.192
S1A Level 7 Roof Garden	65.00 ± 3.00	17878.179
Jun Rui's Home	65.00 ± 3.00	12219.345
MBS Observation Deck	195.00 ± 3.00	5695.627

Data Collection (Additional)

At the Marina Bay Sands Observation Deck, three additional datasets were collected. In two sets, the CosmicWatch was wrapped in Aluminium Foil as shown in Figure 4A. In the third set, a ziplock bag filled with water was set atop the Aluminium Shielded CosmicWatch as shown in Figure 4B. These three datasets were collected to check if shielding would have any significant effect on the count and rate.

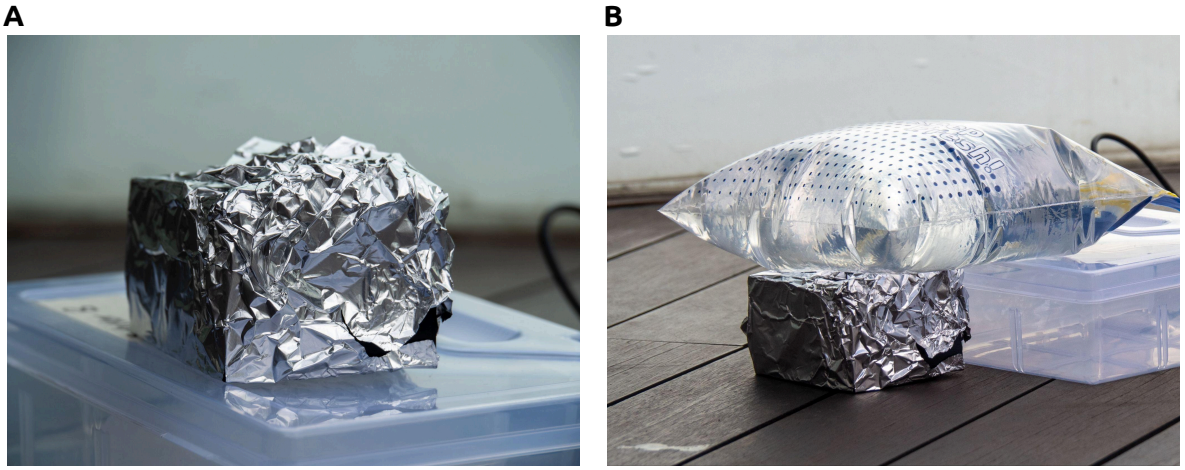

Figure 4: (**A**) Aluminum shielded CosmicWatch and (**B**) Aluminum and water shielded CosmicWatch, during data collection at the Marina Bay Sands Observation Deck.

Mathematical formulation

Assuming the muons have a constant rate of decay, the decay equation can be written as a differential equation,

$$\frac{dN(t)}{dt} = -\lambda N(t) \tag{1}$$

Where $N(t)$ is the number of muons after time t has passed, and λ is the exponential decay constant. Solving this differential equation with the initial condition $N(0) = N_0$, where N_0 is the number of muons at time $t = 0$, we obtain the following decay equation.

(2)

In muon's rest frame, the mean muon lifetime, $\tau = 2.1969811(22) \times 10^{-6}$s.[3] Mean muon lifetime is related with the exponential decay constant by $\tau = \lambda^{-1}$, and thus equation (2) can be rewritten as,

$$N(t) = N_0 \exp\left(\frac{-t}{\tau}\right) \tag{3}$$

In our experiment, we are measuring the count rate, which is the number of muons detected per unit time. Therefore, we can rewrite equation (3) in terms of counts,

$$R(t) = R_0 \exp\left(\frac{-t}{\tau}\right) \tag{4}$$

In terms of our experiment, $R(t)$ is the count rate measured at a level L_E, R_0 is the count rate measured at an elevation of L_0, and t is the time taken for the muon to cover the distance $L_0 - L_E$.

Regardless of whether relativistic effects are true or not, the time taken by the muons to travel a distance $L_0 - L_E$ in their reference frame is given by,

$$t = \frac{L_0 - L_E}{v} \tag{5}$$

Where v is the speed of the muons. Therefore, we can rewrite equation (4) as,

$$R(v, L_E) = R_0 \exp\left(\frac{-(L_0 - L_E)}{v\tau}\right) \tag{6}$$

Assuming no relativistic effects

Equation (6) can be rewritten as,

$$R_N = R_0 \exp\left(\frac{-(L_0 - L_E)}{v\tau}\right) \tag{7}$$

Where R_N is the count rate at the ground assuming no relativistic effects. From equation (7), the speed can be written as the following function,

$$v = \frac{-(L_0 - L_E)}{\ln\left(\frac{R_N}{R_0}\right)\tau} \tag{8}$$

Assuming relativistic effects

According to Special Relativity, particles moving close to the speed of light experiences time dilation (equation (8)) and length contraction (equation (9)) as shown below,

$$T = \frac{T_0}{\sqrt{1 - v^2/c^2}} \tag{9}$$

$$D = D_0\sqrt{1 - v^2/c^2} \tag{10}$$

Where T_0 is the time measured in muon's reference frame, T is the time measured in the Earth's reference frame, D is the distance traveled by the muon in its reference frame, D_0 is the distance traveled in the Earth's reference frame, v is the speed of the muon, and c is the speed of light. In our frame of reference, the muon will have a dilated mean life, τ_D,

$$\tau_D = \frac{\tau}{\sqrt{1 - v^2/c^2}} \tag{11}$$

Therefore, equation (6) can be rewritten as,

$$R_E = R_0 \exp\left(\frac{-(L_0 - L_E)\sqrt{1 - v^2/c^2}}{v\tau}\right) \tag{12}$$

Where R_E is the count rate measured at the ground accounting for relativistic effects. Therefore, the velocity can be written as,

$$v = \left\{\left[\frac{\tau}{(L_0 - L_E)}\ln\left(\frac{R_E}{R_0}\right)\right]^2 + \frac{1}{c^2}\right\}^{-1/2} \tag{13}$$

Results

Table 2 shows the data fields collected by the CosmicWatch Muon detector.

Data collection was conducted across multiple days throughout the day. Specifications of each of the data bins is summarized in Table 3.

From the data, preliminary results were obtained. Detection rates from each collection bins were calculated from total detector uptime (Ardn_time – Deadtime) of each data point in each data bin.

Performing a linear regression on the complete dataset shows that the count rate remains fairly constant throughout the data collection process, with a Pearson correlation coefficient extremely close to 1.000.

Table 2: Data fields collected by CosmicWatch and the meaning of each field.

Data fields	Meaning
`Event`	Muon detection event
`Ardn_time[ms]`	Total elapsed Arduino uptime when event was recorded
`ADC[0-1023]`	Signal peak value from Analog-to-Digital converter
`SiPM[mV]`	SiPM peak voltage calculated from ADC value; proportional to the number of photos triggering the SiPM
`Deadtime[ms]`	Total dead-time of the detector
`Temp[C]`	Measured temperature of the detector

Table 3: Preliminary experimental data collected in various locations

Height [m]	Rate [s^{-1}]	Count	r^2 Correlation	Data bin
4.00 ± 0.50	0.786±0.001	962	0.999	utown_green_1
4.00 ± 0.50	0.884 ±0.001	1227	1.000	utown_green_2
4.00 ± 0.50	0.803 ±0.001	1021	1.000	utown_green_3
4.00 ± 0.50	0.593 ±0.000	8422	1.000	utown_green_4
15.00 ± 3.00	0.850 ±0.001	1157	1.000	mbs_ground_1
15.00 ± 3.00	0.734 ±0.001	1048	0.999	mbs_ground_2
65.00 ± 3.00	0.674 ±0.000	10451	1.000	S1A
65.00 ± 3.00	0.554 ±0.000	2887	1.000	HDB_1
65.00 ± 3.00	0.539 ±0.000	3685	1.000	HDB_2
195.00 ± 3.00	0.529 ±0.001	830	1.000	mbs_shielded_1
195.00 ± 3.00	0.546 ±0.001	569	0.999	mbs_shielded_2
195.00 ± 3.00	0.488 ±0.001	709	0.999	mbs_unshielded
195.00 ± 3.00	0.478 ±0.001	779	0.999	mbs_water

Curiously, the recorded count rates for lower elevations consistently appear higher than the count rate recorded at the Marina Bay Sands observation deck (195.00 ± 3.00)m. This contradicts the expected results, as the observed count rate should decrease with decreasing elevation.

The anticipated trend is based on the assumption that muons will undergo decay over time as they travel from the atmosphere to ground level.

The anomalous data observed can be elucidated through Figure 5, wherein a comprehensive analysis of events within the entire dataset reveals a notable increase in count for events characterized by SiPM pulse amplitudes smaller than 30mV. According to the reference paper on CosmicWatch, authored by Axani et al., such low SiPM pulse amplitudes are indicative of false positives stemming from background radiation sources.

Axani et al. employed a coincidence measurement setup in their reference paper, where coincidental measurements were categorized as positives, and independent events were labeled as false positives. In this setup, false positive triggers could be effectively filtered and excluded from the dataset. Unfortunately, due to the constraint of having only one operational muon detector, implementing a coincidental setup was unfeasible for our experiment.

It is noteworthy that prior research groups did not encounter the anomalous data readings observed in our study. This divergence can be traced back to our group's flashing and reprogramming of the on-board Arduino Nano chip without subsequent calibration to known sources or calibrated lab-controlled signals.

Despite these challenges, our data analysis can be refined by selecting a subset of the dataset. Specifically, we opt for data points with ADC values smaller than 128. This targeted subset allows us to mitigate the impact of anomalous false positives originating from background radiation, thereby enhancing the reliability of our data analysis in the context of our research.

Selecting a subset of the dataset for analysis will not affect the accuracy of our results as comparing the histogram counts from each data set, we see that each subset counts are proportional to each other.

From Figure 5C, we observe that SiPM values of lower than 30mV correspond to the range of ADC values smaller than 128. Consequently, an ADC value smaller than 128 was selected as the lower threshold for the subset of data utilized in the analysis.

Data after filtering with ADC>128 parameter is summarized in Table 4.

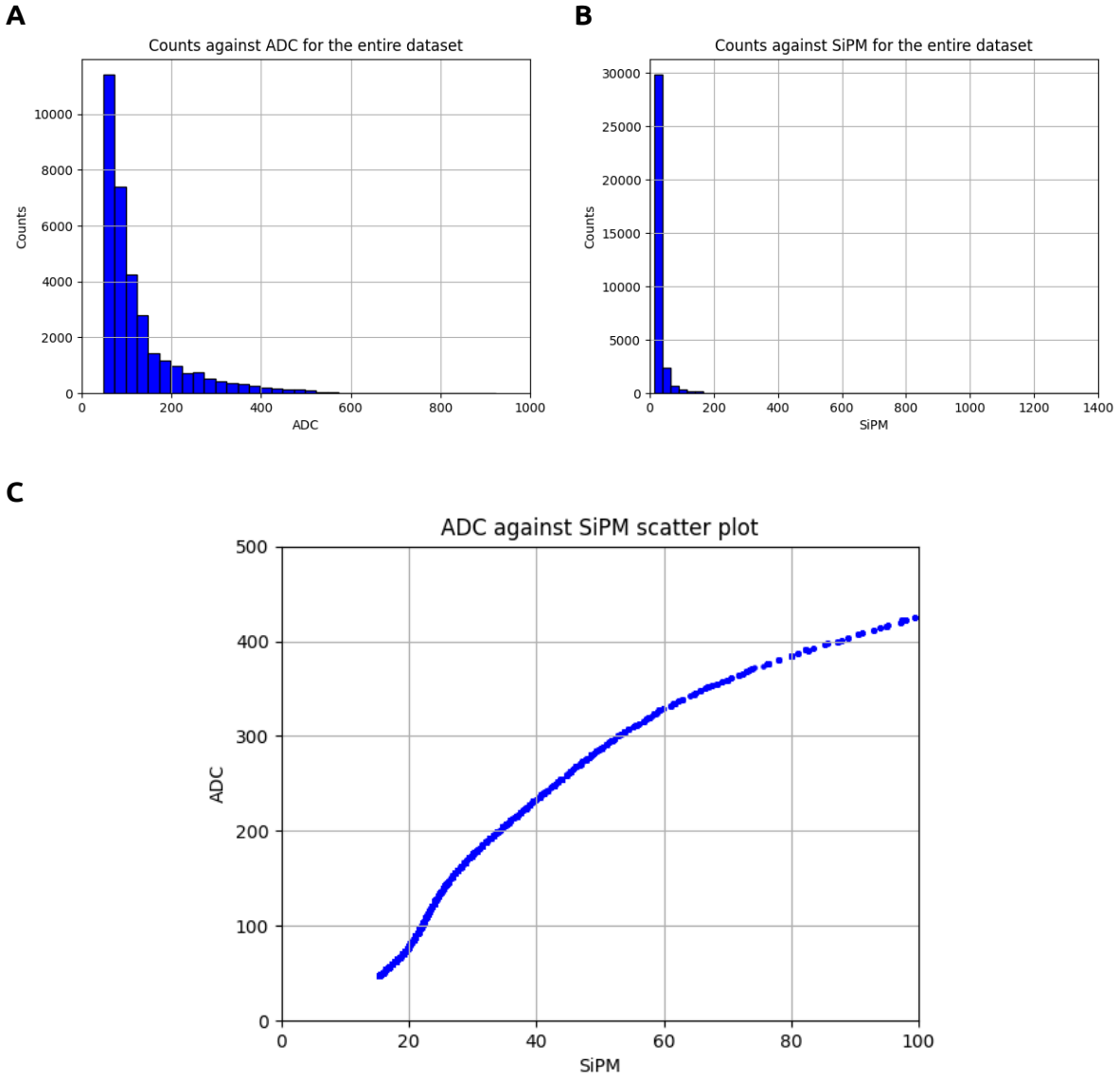

Figure 5: (**A**) Counts against ADC and (**B**) counts against SiPM for the entire dataset, showing how the data is heavily right skewed. (**C**) shows the ADC against SiPM. When SiPM is 30mV, the ADC is 128.

Table 4: Filtered experimental data from various locations

Height [m]	Rate [s^{-1}]	Count	r^2 Correlation	Data bin
4.00 ± 0.50	0.234 ±0.001	289	0.997	utown_green_1
4.00 ± 0.50	0.237 ±0.000	345	0.999	utown_green_2
4.00 ± 0.50	0.205 ±0.001	264	0.999	utown_green_3
4.00 ± 0.50	0.169 ±0.000	2414	0.999	utown_green_4
15.00 ± 3.00	0.249 ±0.001	336	0.998	mbs_ground_1
15.00 ± 3.00	0.238 ±0.001	352	0.998	mbs_ground_2
65.00 ± 3.00	0.173 ±0.000	2699	1.000	S1A
65.00 ± 3.00	0.158 ±0.000	820	1.000	HDB_1
65.00 ± 3.00	0.154 ±0.000	1044	1.000	HDB_2
195.00 ± 3.00	0.206 ±0.000	322	0.999	mbs_shielded_1
195.00 ± 3.00	0.202 ±0.001	212	0.998	mbs_shielded_2
195.00 ± 3.00	0.188 ±0.000	267	0.999	mbs_unshielded
195.00 ± 3.00	0.202 ±0.000	329	0.999	mbs_water

Table 5: Averaged muon event count rates in each location

Location	Height [m]	Average Rate [s^{-1}]
UTown Green	4.00 ± 0.50	0.211 ± 0.001
MBS Ground	15.00 ± 3.00	0.244 ± 0.001
S1A	65.00 ± 3.00	0.173 ± 0.000
HDB	65.00 ± 3.00	0.156 ± 0.000
MBS Observation Deck	195.00 ± 3.00	0.200 ± 0.000

Discussions

Throughout this section, we take R_0 to be the count rate corresponding to collection bins obtained at Marina Bay Sands observation deck (195.00 ± 3.00)m.

Non-Relativistic v.s. Relativistic conditions

For our preliminary analysis, we take the average speed of muons to be $v = (0.9952 \pm 0.002)c$.[3] Comparing the expected muon count rates (Table 6) to the observed muon count rates at various elevations (Table 5), we observe that the expected count rates contradict the counts collected at lower elevations. Specifically, each of the count rates collected at elevations lower than $L_0 = 195.00\,m$ observed higher count rates compared to the predicted count rates.

Table 6: Predicted count rates with $R_0 = 0.200$

Height [m]	Predicted count rates (non-relativistic)	Predicted count rates (relativistic)
195.00	0.200	0.200
65.00	0.164	0.196
15.00	0.152	0.195
4.00	0.148	0.194

On the contrary, when we account for the time dilation effects foreseen by Einstein's Special Theory of Relativity, we notice that the newly predicted count rates align more closely with the range of count rates observed at each elevation. Consequently, we will focus solely on the relativistic cases.

Shielding

Here, we perform a single factor ANOVA test to determine if there are significant differences between the 4 sets of data collected (2 for shielded, 1 for unshielded and 1 for shielded with a water bag set atop of it).

We obtained a p-value of 1.50×10^{-31}. Apart from the incredibly low p-value being a likely result of the large data set (~1000 points), since it is less than or equal to 0.0005, we reject the null hypothesis (difference in sample means is 0) at a 0.05% significance level and conclude that there is sufficient evidence to suggest that the difference in sample means is different from zero and thus the *event* count rates measures with different shieldings applied differ from each other.

Additionally, we performed a Tukey's honestly significant difference (HSD) test (Table 7) to ensure that in a pairwise comparison, the mean *event* count rates are significantly different from each other.

Table 7: Tukey's Honestly significant difference pairwise group comparison (0 – Shielded 1; 1 – Shielded 2; 2 – Unshielded; 3 – Shielded + Water)

Comparison	Test statistic	p-value
0 – 1	-0.004	0.077
0 – 2	0.003	0.278
0 – 3	-0.015	0.000
1 – 2	0.007	0.001
1 – 3	-0.011	0.000
2 – 3	-0.018	0.000

At 5% significance level, we can conclude that the mean *event* count rate for the shielded 1 dataset is significantly different from that of the shielded 2 dataset and unshielded dataset. Thus, our conclusion is likely to be free from a type I error for those 2 pairwise comparisons and thus we can reject the null hypothesis, that the difference between sample mean *event* count rates is 0, and conclude that adding shielding does have a significant effect on the *event* count rate.

However, it is peculiar to why we only observe significant differences between shielded 1, shielded 2 and unshielded data sets. Whereas, the shielded + water data set exhibited no significant differences from the mean in a Tukey's Honestly significant difference pairwise test.

Although we are able to arrive at the aforementioned conclusion from a statistical test, it is imperative for us to understand the environment our test was conducted in. We acknowledge the high collection-to-collection variability across all of the data we have collected. This is likely a result of abnormally high false positive events triggered by the SiPM. The nature of the shielding might therefore reduce the false positive event rate, while not reducing the muon incident rate. Improvements to the testing process, calibration, and further testing will thus be necessary to determine if shielding has an effect on muon incident rate on the sensor or if it just simply reduces false positive event rates.

Therefore, although we can conclude from our data that statistically, the mean *event* count rate does significantly differ depending on the shielding used on the detector, further testing is needed to arrive at a more conclusive result.

Comparing the expected and observed rates

As seen in Table 8, as elevation increases, the predicted count rate increases. However, this is not observed in the observed count rate. UTown Green and MBS Ground, are in fact higher than the MBS Observation Deck, which should not be the case.

Table 8: Observed and predicted muon count rates comparison at various elevations

Location	Elevation [m]	Observed Rate [s^{-1}]	Predicted Rate [s^{-1}]
UTown Green	4.00 ± 0.50	0.211 ± 0.001	0.194
MBS Ground	15.00 ± 3.00	0.244 ± 0.001	0.195
S1A	65.00 ± 3.00	0.173 ± 0.000	0.196
HDB	65.00 ± 3.00	0.156 ± 0.000	0.196
MBS Observation Deck	195.00 ± 3.00	0.200 ± 0.000	0.200

Here we propose a few plausible reasons as to why we observe such unexpected rates.

As explained in the results section earlier, the sensor was not calibrated using a coincidence sensor. This implies that there could be multiple false positives in our data set, which causes the count to increase, and hence we observe a higher than expected rate.

Moreover, the cloud cover was 100% during the data collection. It has been observed that muons could lose energy after moving through the electric field of clouds.[8] This implies their speed will decrease, and they will decay at a greater elevation, reducing the count rate observed at top of Marina Bay Observation Deck.

The higher count rate at the ground level could also be due to commercially available sources of radiation, as mentioned by Axani et al. in their supplementary physics paper. One material that stands out is granite, which was in fact present in large quantities when data collection took place at UTown Green and at the ground level of Marina Bay Sands. This could have increased the count rate.

Phenomenological model for muon average velocities

When high-energy cosmic rays, predominantly composed of protons and atomic nuclei, penetrate the Earth's atmosphere, a sequence of interactions ensues, giving rise to a cascade of secondary particles. Among these secondary particles are pions, short-lived particles resulting from the collisions. As the pions rapidly decay, muons, akin to electrons but considerably more massive, are generated.

Despite their limited lifespan, muons can reach the Earth's surface before undergoing decay, a phenomenon facilitated by the time dilation effects predicted by special relativity. From the previous sections, we concluded that relativistic effects do affect the decay of muons created from cosmic ray interactions falling down to the Earth’s surface. As such, we construct a phenomenological model to model the decay of muons.

We plotted a graph of R_E normalized with respect to R_0 for different elevations using equation 12 as seen in Figure 6. The values of v were in terms of speed of light c.

As seen from the graph in Figure 6, experimental data obtained matches with some of the data points well. Suggesting that the velocity of muons range between 0.50c and 1.00,, similar to the values reported in similar literature.[2,3,4] Possible reasons as to why we have observed *superluminal* muon average velocities have been explained in the previous

sections. We acknowledge that there are likely significant vertical error bars that are not easily quantifiable but present due to significant background false positive events and imprecise calibration of the detector.

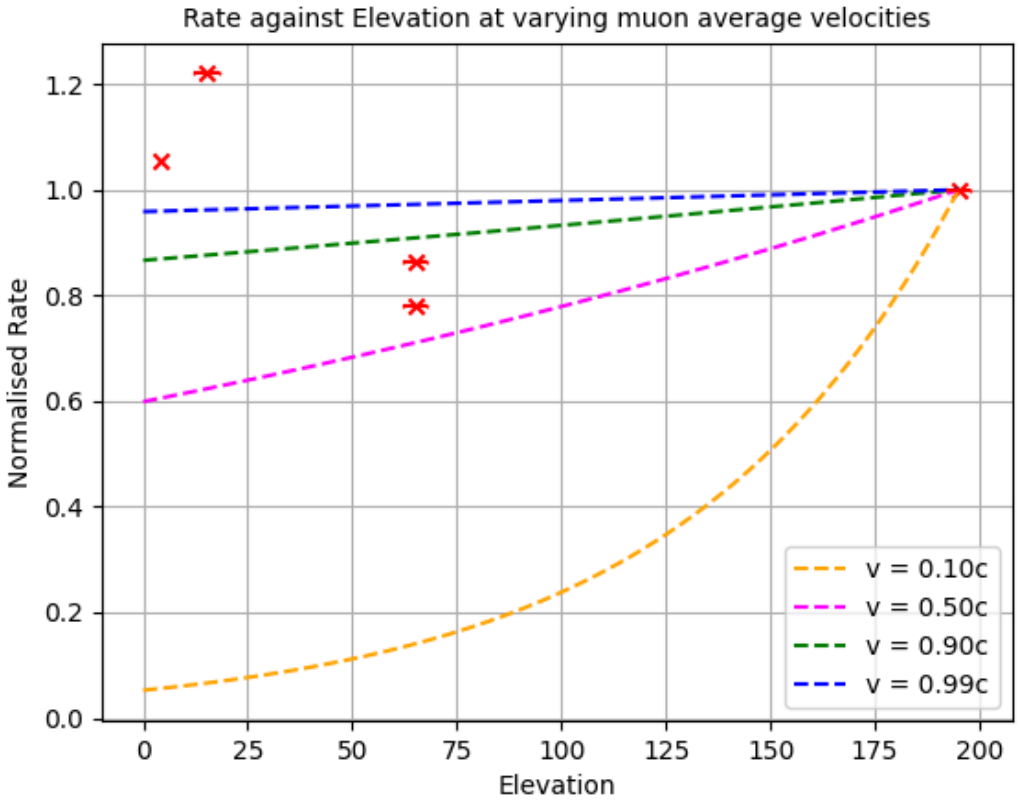

Figure 6: Graph of Rate (normalized with respect to R_0) against Elevation for different values of v (in units of speed of light c). Red points indicate experimentally derived rates at various elevations. The various curves correspond to various muon average velocities in units of c, and the expected rates through various elevations from decay.

Velocity Determination & Error Analysis

We have adopted to quantify errors from count rate collection using a simple linear regression instead of modeling the decay as a Poissonian distribution as detailed in the reference paper.

It is known that a Poisonnian distribution would describe the distribution of count rates well only when the size of the data set approaches infinity. However, in our case of an experimental phenomenological study, it would be far more accurate to model the error of

the instrument and collection through a linear regression which would directly give the standard error and deviation of a spread of a data from its best-fit line.

Regardless, we have included the alternative count rate error model (Poisonnian) in the Appendix.

From equation (13), we get the error propagation for the velocity of muon:

$$\frac{\Delta v}{v} = \sqrt{(\frac{\delta \tau}{\tau})^2 + (\frac{\delta L_0}{L_0})^2 + \frac{(\frac{\delta R_E}{R_E})^2 + (\frac{\delta R_0}{R_0})^2}{[ln(\frac{R_E}{R_o})]^2}} \tag{14}$$

The derivation of equation (14) is as follows:

$$\delta \frac{R_E}{R_0} = \frac{R_E}{R_0} \sqrt{(\frac{\delta R_E}{R_E})^2 + (\frac{\delta R_0}{R_0})^2} \tag{15}$$

$$\delta\ ln(\frac{R_E}{R_0}) = \frac{R_0}{R_E}\ \delta \frac{R_E}{R_0} \tag{16}$$

Substitute equation (15) into equation (16),

$$\delta\ ln(\frac{R_E}{R_0}) = \sqrt{(\frac{\delta R_E}{R_E})^2 + (\frac{\delta R_0}{R_0})^2} \tag{16}$$

Let $Y = \frac{\tau}{L_0} ln(\frac{R_E}{R_0})$, $\Delta L\ = L_0 - L_{E'}$ then

$$\delta \frac{\tau}{\Delta L} = \frac{\tau}{\Delta L} \sqrt{(\frac{\delta \tau}{\tau})^2 + (\frac{\delta \Delta L}{\Delta L})^2} \tag{17}$$

The error propagation of velocity v is then

$$\begin{aligned}\frac{\Delta v}{v} &= \frac{\Delta v^2}{2v^2} \\ &= \frac{1}{2}\sqrt{(\frac{\delta Y^2}{Y^2})^2 + 0} \\ &= \frac{1}{2}\frac{\delta Y^2}{Y^2} \\ &= \frac{\delta Y}{Y}\end{aligned} \tag{18}$$

Substitute equation (17) into equation (18),

$$\frac{\delta Y}{Y} = \sqrt{(\frac{\delta \frac{\tau}{\Delta L}}{\frac{\tau}{\Delta L}})^2 + [\frac{\delta ln(\frac{R_E}{R_0})}{ln(\frac{R_E}{R_0})}]^2} \tag{18}$$

Thus,

$$\begin{aligned}\frac{\Delta v}{v} &= \frac{\delta Y}{Y} \\ &= \sqrt{[(\frac{\delta \tau}{\tau})^2 + (\frac{\delta \Delta L}{\Delta L})^2] + \frac{(\frac{\delta R_E}{R_E})^2 + (\frac{\delta R_0}{R_0})^2}{[ln(\frac{R_E}{R_o})]^2}}\end{aligned} \tag{14}$$

Equation (14) is used to find the error propagation of the velocity of muon by substituting the values of v at different elevations (Table 9).

The experimentally determined velocities vary greatly. However, this was expected from the previous discussion, where we established that the data collected had significant background false positive events and that there were other factors that introduced variability.

It is important to note that regardless, none of the velocities exceed the speed of light. This shows that the phenomenological model we have constructed to model and account for the average velocity of muons have prevented ‘superluminal’ predictions. Additionally, under a Lorentzian transformation, values greater than c will result in a complex term.

Table 9: Experimentally determined average muon velocities at various elevations

Location	$\delta\tau$ **/** τ	$\delta\Delta L$ **/** ΔL	**Δv [ms^{-1}]**	**Velocity, v [c]**
UTown Green	1.00×10^{-8}	0.125	2.611×10^{7}	0.983
MBS Ground	1.00×10^{-8}	0.200	6.426×10^{7}	0.809
S1A	1.00×10^{-8}	0.0462	5.575×10^{7}	0.806
HDB	1.00×10^{-8}	0.0462	4.303×10^{7}	0.622

Conclusion

Preliminary results indicated a deviation from the expected count rates, with lower elevations showing unexpectedly higher counts. Several factors such as false positives from background radiation, lack of coincidence measurement setup, and uncalibrated sensor contributed to these anomalies.

The statistical analysis of shielding effects revealed significant differences between shielded and unshielded datasets, emphasizing the need for further testing to understand the impact of shielding on muon incident count rates and false positive reduction. Despite challenges, the experiment provided valuable insights into relativistic effects on muon decay, suggesting the need for improved calibration and experimental setups for accurate results.

Limitations in the experiment, including false positives and lack of calibration, highlight the need for caution in interpreting the results. Future extensions could involve refining the experimental setup, implementing coincidence measurement, and addressing environmental factors affecting muon behavior. Additionally, exploring the impact of cloud cover and commercial radiation sources on muon decay rates could contribute to a more comprehensive understanding.

In conclusion, while the experiment faced challenges and limitations, it contributes valuable insights into the complexities of measuring relativistic effects on muons. Addressing these limitations and conducting further experiments will enhance the accuracy and reliability of the results, advancing our understanding of relativistic phenomena in particle physics.

Again, we would like to extend our sincerest thanks and gratitude for the mentorship and guidance from **A/Prof. Phil CHAN Aik Hui**, **Mr. KUANG Jianhong**, and the Department of Physics at the National University of Singapore.

References

(1) Einstein, A. Zur elektrodynamik bewegter Körper. *Annalen der Physik* **322**, 891–921 (1905).

(2) Rossi, B. & Hall, D. B. Variation of the rate of decay of mesotrons with momentum. *Physical Review* **59**, 223–228 (1941).

(3) Olive, K. A. Review of Particle Physics. *Chinese Physics C* **40,** 1–1808 (2016).

(4) Axani, S. N., Frankiewicz, K. & Conrad, J. M. The COSMICWATCH Desktop Muon Detector: A self-contained, pocket sized particle detector. *Journal of Instrumentation* **13,** (2018).

(5) Axani, S. N. The Physics Behind the CosmicWatch Desktop Muon Detectors. *arXiv* (2019).

(6) Vieyra Software. Physics Toolbox Suite. *Vieyra Software* (2023).

(7) National Archives of Singapore. Singapore Topographical Map. *Singapore Topogrpahical Map* (2014).

(8) Chilingarian, A., Hovsepyan, G., Karapetyan, G. & Zazyan, M. Stopping muon effect and estimation of intracloud electric field. *Astroparticle Physics* **124**, (2021).

Appendix

To calculate the error propagation for the count rate R, suppose the detection of particles in CosmicWatch can be modeled as a Poisson process because it is an exponential decay. This means that the mean is equal to the variance. The mean of a count, is the count itself. This implies the variance is equal to the count. The total variance is equal to the sum of individual variances and therefore, the total variance is equal to the total count. Therefore, the error in count, C,

$$\Delta C = \sqrt{C}$$

Therefore, for the rate, R,

$$\Delta R = \frac{\sqrt{C}}{P}$$

Where P is the period for which the data was calculated. Table 10 details the error calculations.

Table 10: error propagation of ΔR

Data bin	Count	Period of Data Collection	Detector deadtime	Muon Count Rate R	ΔR	Sum of error
utown_green_1	289	1222.576	17.355	0.234	0.014	0.023
utown_green_2	345	1408.235	22.235	0.237	0.013	
utown_green_3	264	1274.445	19.261	0.205	0.013	
utown_green_4	2414	14419.491	155.669	0.169	0.003	
mbs_ground_1	336	1369.092	21.160	0.249	0.014	0.019
mbs_ground_2	352	1414.187	19.172	0.238	0.013	
S1A	2699	17871.782	1981.883	0.173	0.003	
HDB_1	820	5218.059	52.637	0.158	0.006	0.007
HDB_2	1044	6962.790	67.376	0.154	0.005	
mbs_shielded_1	322	1619.860	15.337	0.206	0.011	0.024
mbs_shielded_2	212	1032.991	10.170	0.202	0.014	
mbs_unshielded	267	1421.019	12.771	0.188	0.012	
mbs_water	329	1598.996	14.401	0.202	0.011	